INTERNATIONAL ATOMIC ENERGY AGENCY
UNITED NATIONS EDUCATIONAL, SCIENTIFIC AND CULTURAL ORGANIZATION
INTERNATIONAL CENTRE FOR THEORETICAL PHYSICS
I.C.T.P., P.O. BOX 586, 34100 TRIESTE, ITALY, CABLE: CENTRATOM TRIESTE

UNITED NATIONS INDUSTRIAL DEVELOPMENT ORGANIZATION
INTERNATIONAL CENTRE FOR SCIENCE AND HIGH TECHNOLOGY
c/o INTERNATIONAL CENTRE FOR THEORETICAL PHYSICS 34100 TRIESTE (ITALY) VIA GRIGNANO, 9 (ADRIATICO PALACE) P.O. BOX 586 TELEPHONE 040-224572 TELEFAX 040-224575 TELEX 460449 APH I

H4.SMR/676-29

# SECOND SCHOOL ON THE USE OF SYNCHROTRON RADIATION IN SCIENCE AND TECHNOLOGY: *"JOHN FUGGLE MEMORIAL"*

**25 October - 19 November 1993**

***Miramare - Trieste, Italy***

## *EXAFS IV*

**A. Fontaine**
**L.U.R.E.**
**Orsay, France**

$Y_1Ba_2Cu_3O_{6+x}$

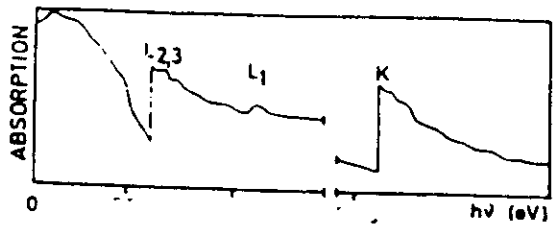


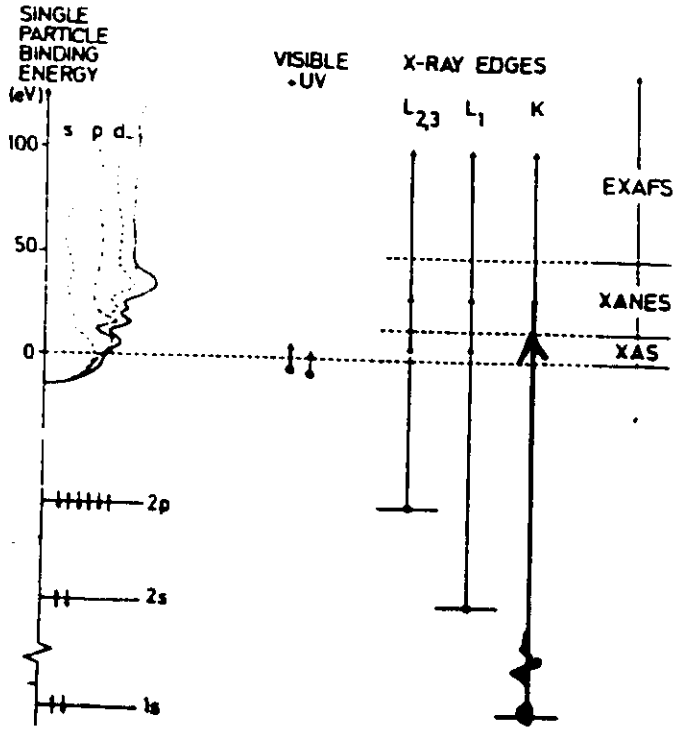


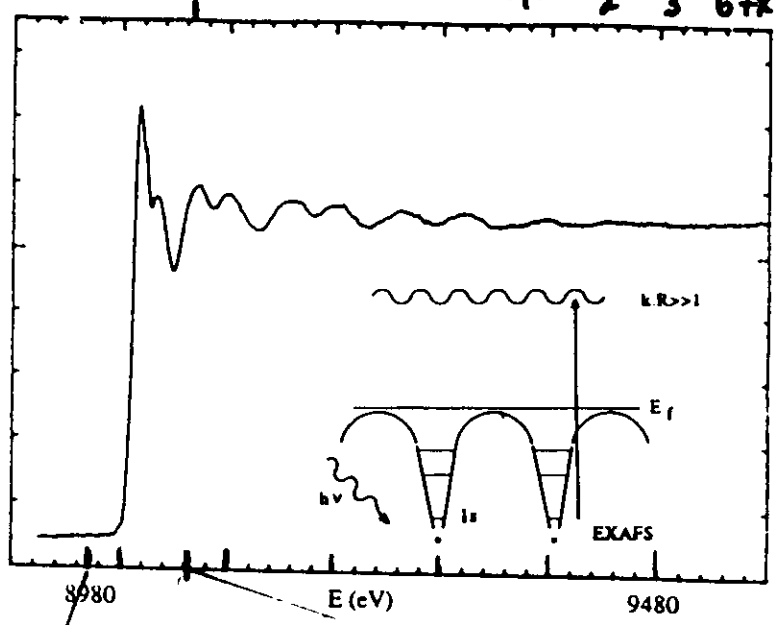


a : Spectre complet d'Exafs où les oscillations s'étendent au-delà de 600 eV après seuil.

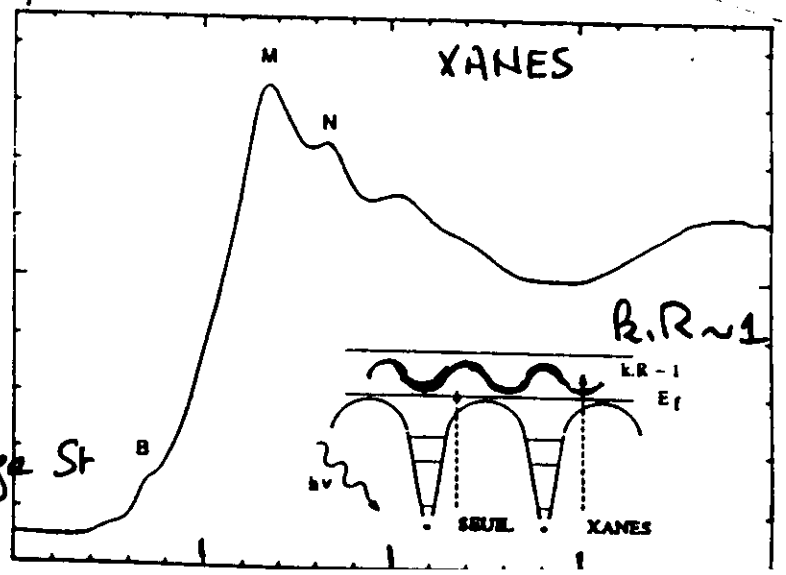


X-ray Absorption Near Edge St

Cu edges XAS.

1. How good is OUR UNDERSTANDING of what we measure?

2. What are the useful informations brought by the DATA.?

3. How accurate are the outputs.

# COPPER EDGES K $L_{III} - L_{II}$

Part of H. TOLENTINO thesis Orsay 1990 / Kosugi, Tranquada with Goddard, Joniach.

$$\mu = \frac{N}{hc}\frac{e^2}{\varepsilon_0}\frac{\omega^3}{\pi}\sum_f |\langle i|\underset{(1)}{}\ \underset{(3)}{\vec{\varepsilon}.\vec{r}}\ \underset{(2)}{|}\underset{(4)}{f}\rangle|^2\ \delta(\omega-\omega_0+\Gamma\nu)$$

## 4 TOOLS

(1) Element selectivity

(2) Selection rules

$|1s^2 \ldots 4p^0\rangle \longrightarrow |1s^1 \ldots 4p^2\rangle$

$2p^{3/2}_{2p^{1/2}}\ |\ldots 2p^6\ldots\rangle \longrightarrow |2p^5\ldots\rangle$ → $3d^{10}\,4s^1$

(3) Linear polarization Anisotropy $Cu^{II}$ (Jahn-Teller)

(4) Core hole

Relaxation involved: localized electrons; photoelectron.

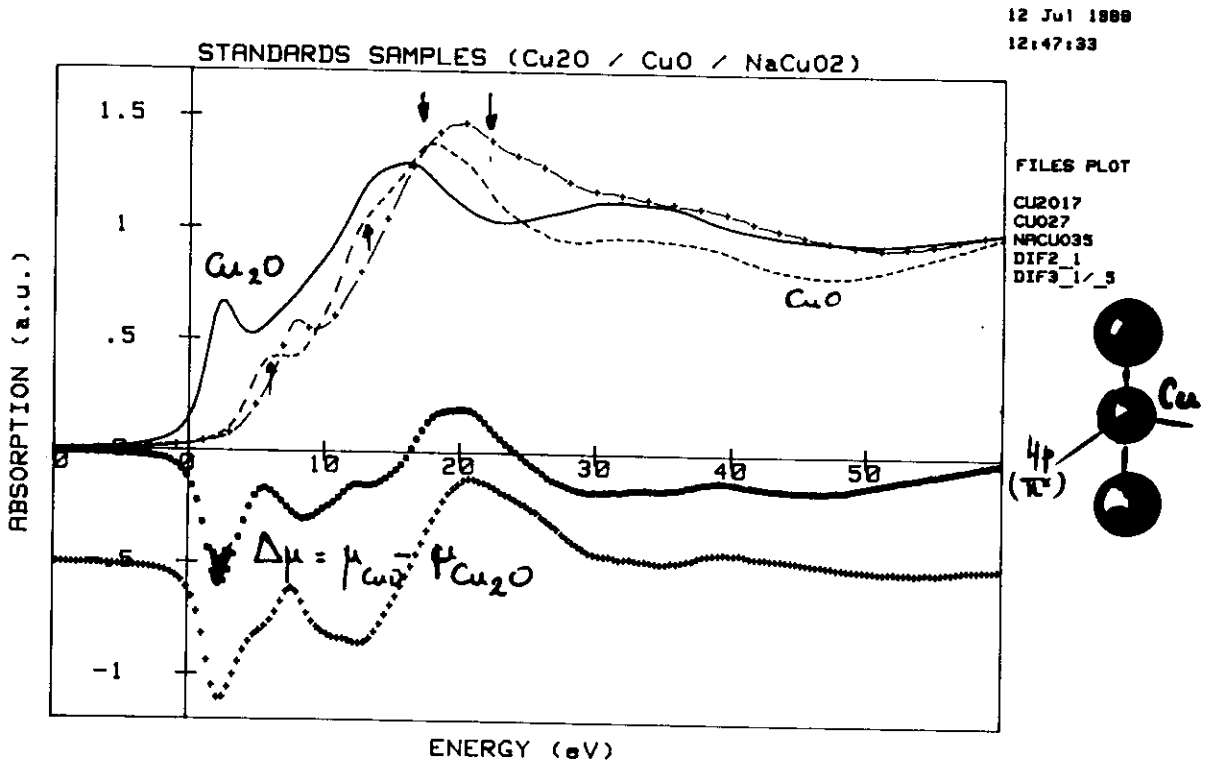


-AN CARRE / SUPRA
Cu I + Cu II Cu III)
hors CHANCE
LINAC / with ARGONITE

Alain 70,120,5,9

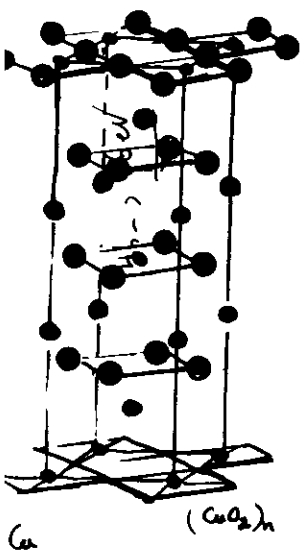


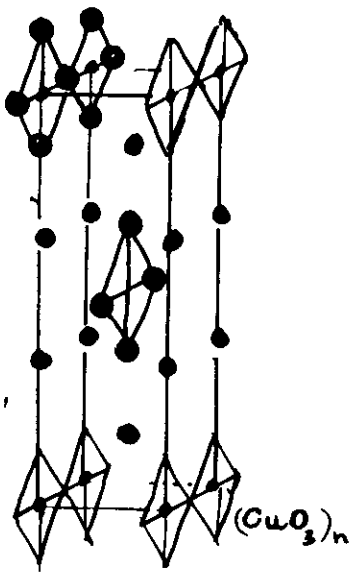


Gd
Nd

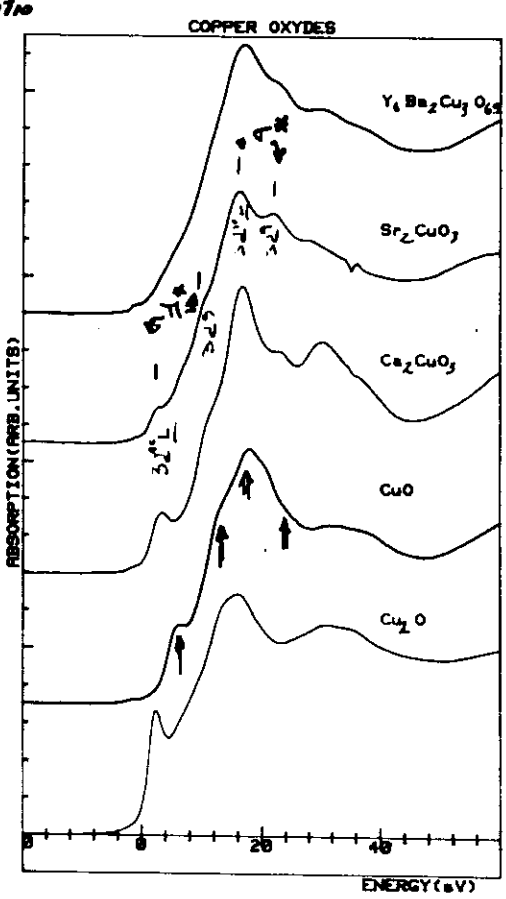


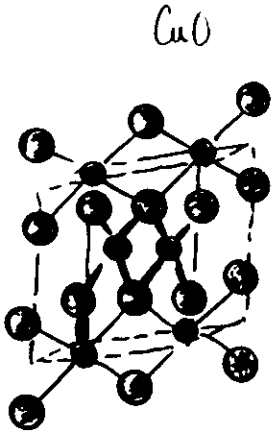


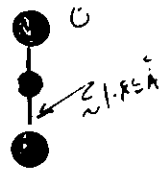

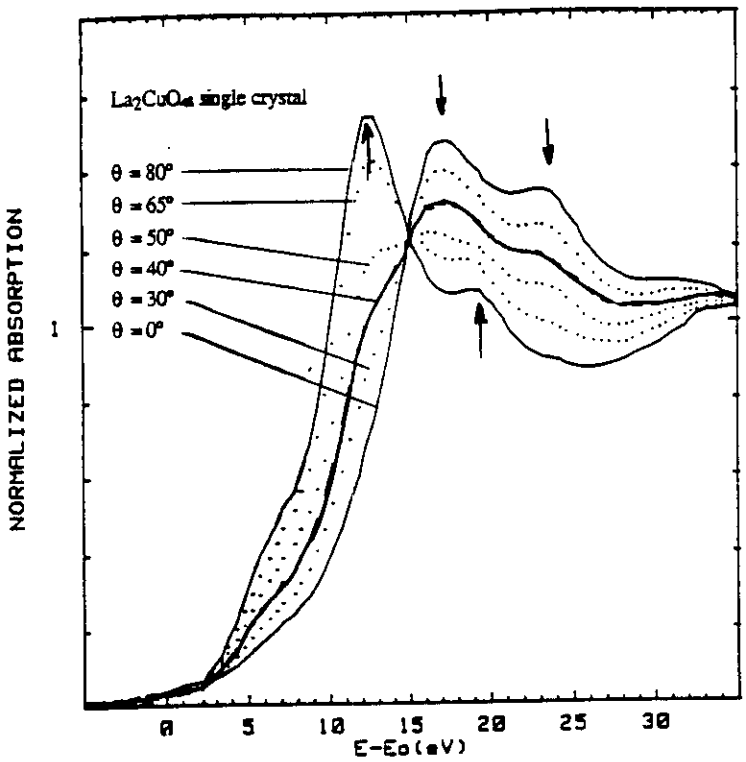


Fig. 2 Angle-resolved Cu K-edge XAS spectra of $La_2CuO_4$ single crystal. Apart from an energy re-scaling to account for differences in next neighbor distances, the anisotropy of the relative intensity of the $3d^{10}\underline{L}$ and $3d^9$ transitions is induced by the symmetry of the photoelectron wavevector k relative to the O $2p_{x,y}$ ligand electron.

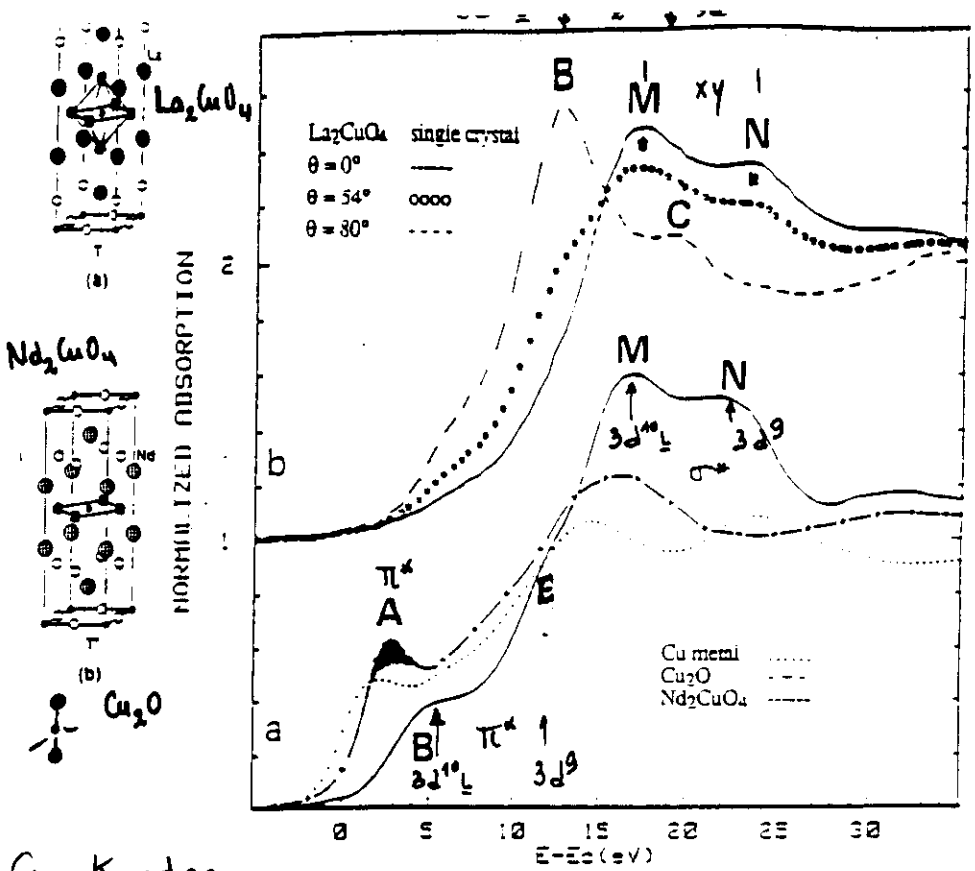


Cu K-edge

- BULK
- IN-SITU
- DISTANCES

$(E-E_0)R^2 = cst$

$XAS \simeq XPS \otimes 4pDOS \otimes (e_k^{\parallel,\perp})$ photoelect.

Table III

Energy positions (in eV) of the main Cu 1s → 4pσ* transitions and corresponding Cu-O distances in Å

| | symmetry | $3d^{10}\underline{L}$ | $3d^9$ | difference | Cu-O distance | $(E-E_0)R^2$ |
|---|---|---|---|---|---|---|
| | | $E_0$ | | | | |
| $Nd_2CuO_4$ | z | 4.6 | 12.0 | 7.4 | - | |
| $Nd_2CuO_4$ | x,y | 16.3 | 22.5 | 6.2 | 1.97 | 45.4 |
| $La_2CuO_4$ | x,y | 17.2 | 23.6 | 6.4 | 1.91 | 46.0 |
| $La_2CuO_4$ | z | 12.5 | 19.6 | 7.1 | 2.45 | 47.4 |
| $YBa_2Cu_3O_7$ | x,y | 17.0 | 23.8 | 6.8 | 1.95 | 47.2 |
| $YBa_2Cu_3O_6$ | x,y | 16.8 | 23.5 | 6.7 | 1.94 | 45.9 |
| $YBa_2Cu_3O_{6.6}$ | x,y | 17.0 | 23.5 | 6.5 | 1.95 | 47.2 |
| $YBa_2Cu_3O_{6.6}$ | z | 18.2 | 24.0 | 5.8 | 1.83 | 45.5 |
| $YBa_2Cu_3O_{6.6}$ | z | 12.5 | - | - | 2.40 | 45.5 |

$W = \left[(u_{cd} - A)^2 + 4t^2\right]^{1/2}$

$46.4 \pm 1$

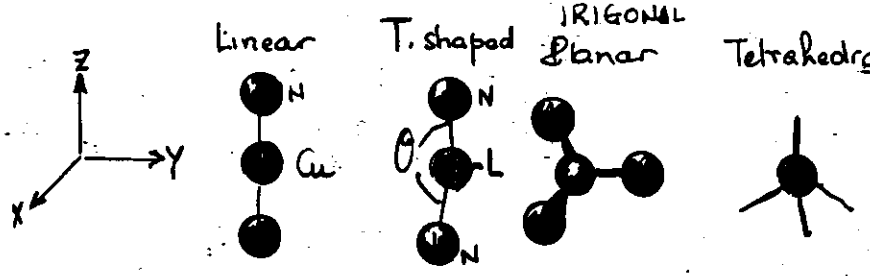


LUNG-SHAN KAU, PENNER-HAHN, SOLOMON, HODGSON

J. Phys C8, n°12 T 47. 1986.

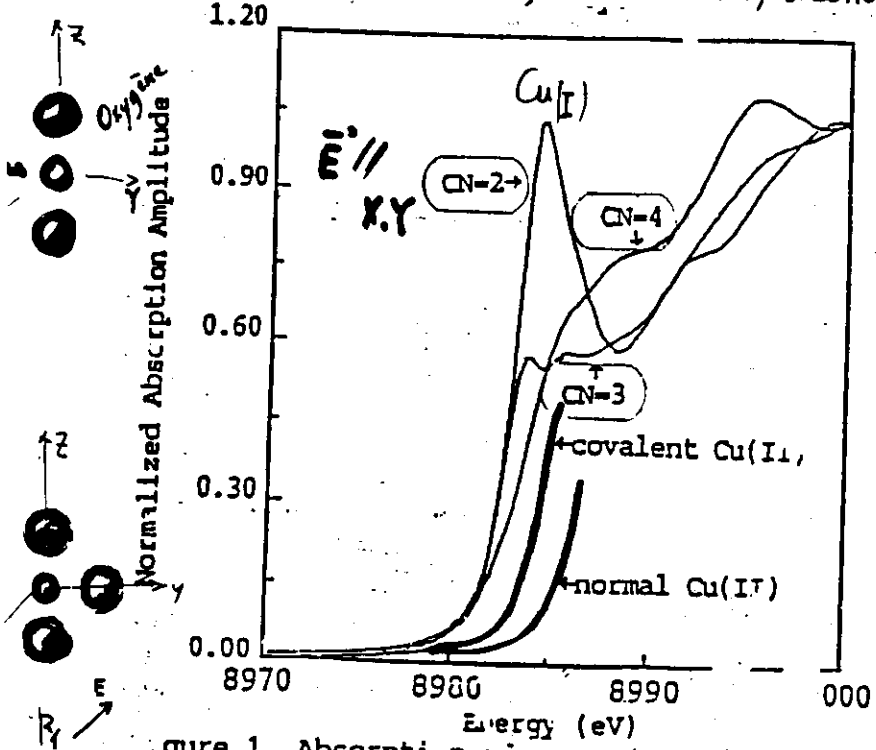


Figure 1. Absorption edge spectra of representative 2-, 3- and 4-coordinate Cu(I) complexes with those of normal and covalent Cu(II) complexes (below 8985.0 eV).

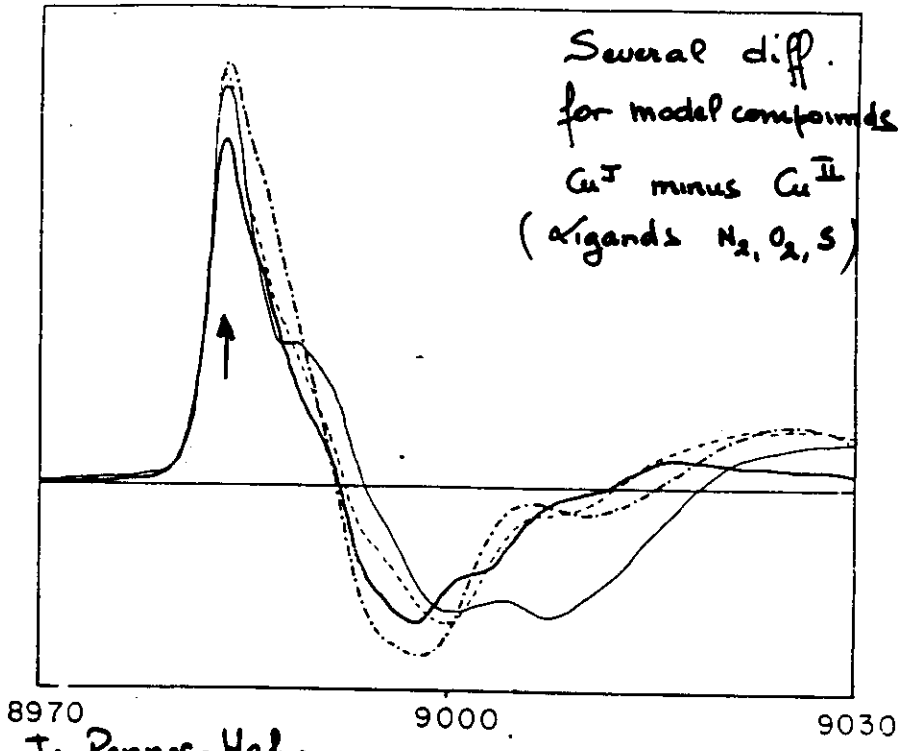


J. Penner-Hahn Thesis Stanford.

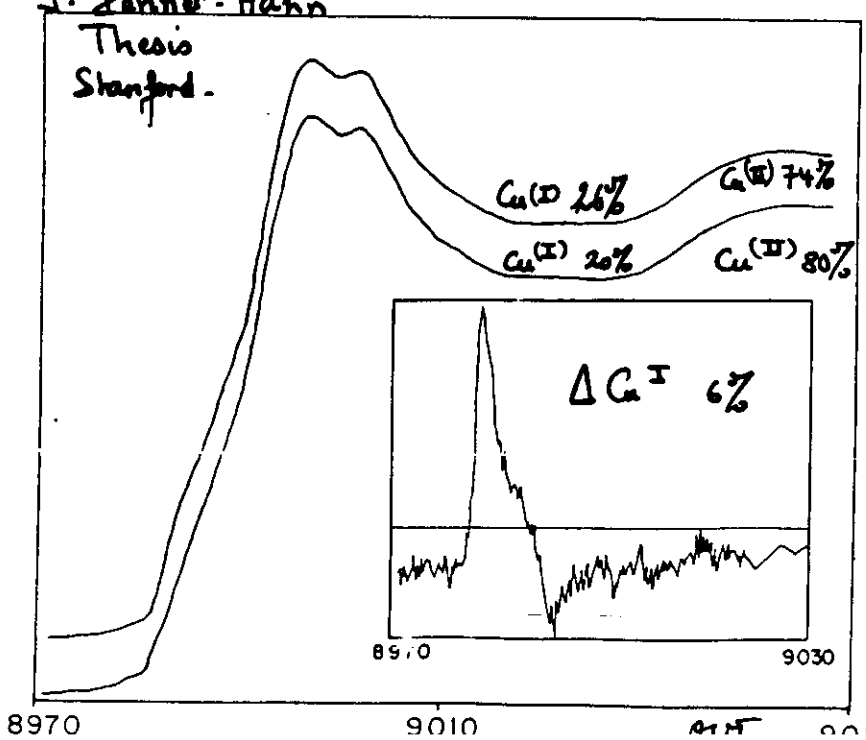

## CUPRATES:

**The picture of the Electronic states:**

**A DOPED CHARGE-TRANSFER INSULATOR**

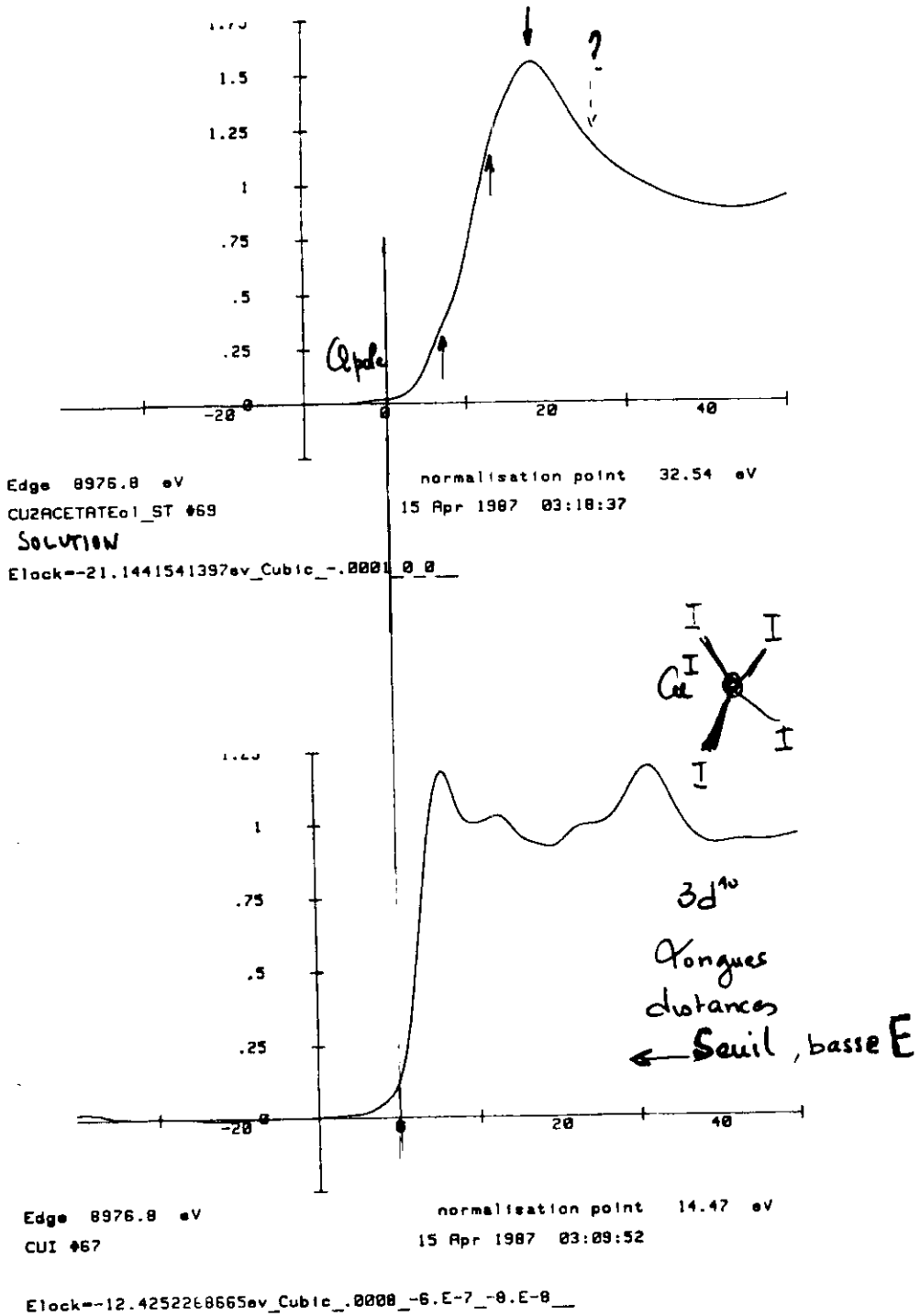

SQUARE PLANAR CUPRATE:

CHARGE TRANSFER INSULATOR

Zaanen, Sawatzky, Allen PRL 85

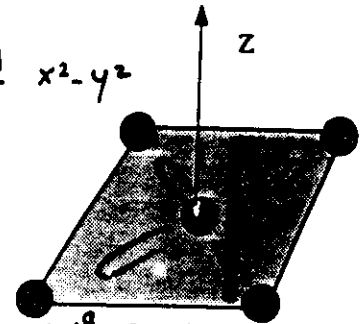


$|Cu, 1s^2 \dots 3d^9; O\ 1s^2 \dots 2p^6\rangle$

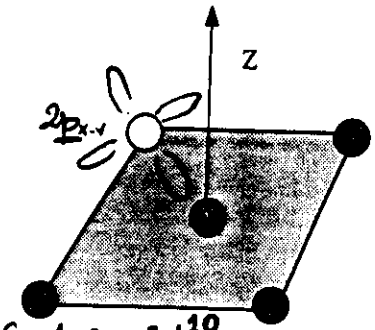


$|Cu, 1s^2 \dots 3d^{10}; O\ 1s^2 \dots 2p^5\rangle$

$d_i^9 d_j^9 \rightarrow d_i^8 d_j^{10}$

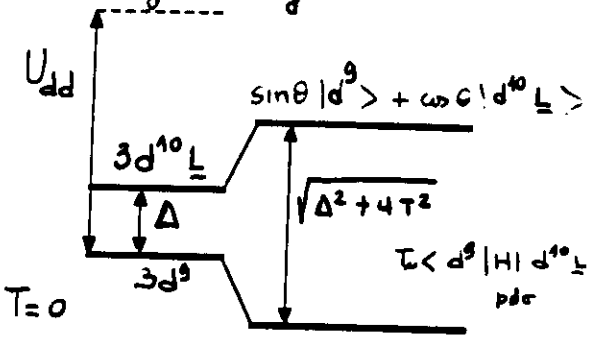


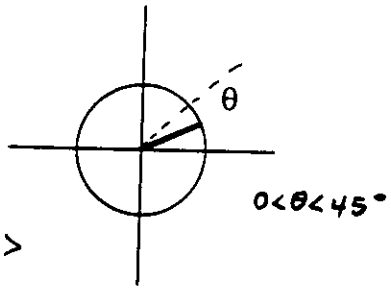


$\boxed{\cos\theta\,|d^9\rangle - \sin\theta\,|d^{10}\underline{L}\rangle}$

$tg\,2\theta = \frac{2T}{\Delta}$

GROUND STATE

$\cos^2\theta \sim 0.67$

$\sin^2\theta \sim 0.33$

$\left\{ \begin{array}{l} T \sim 2\,eV \\ \Delta \sim 1.5\,eV \end{array} \right.$

$U_{dd} \gg \Delta$

Charge-Transfer Semiconductors

$CuCl_2$, $CuBr_2$, CuO, $NiCl_2$ ---

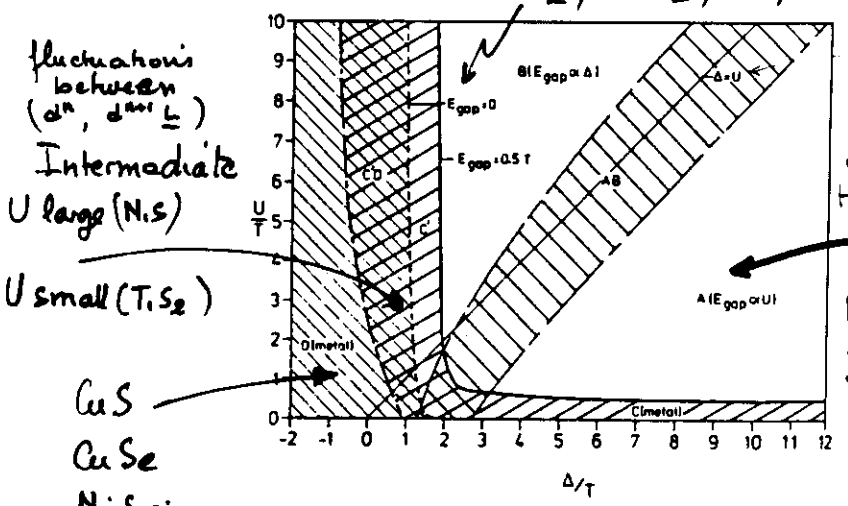


FIG. 3. A phase diagram exhibiting the various regions discussed in the text. The heavy solid line is the semiconductor-metal separation line.

- Superconductivity
- Magnetism
- Reactivity
- Heavy fermions

The **Cu K-edge** Absorption Spectroscopy:

- **Ground states.**

**Cu (I)** as $|1s^2 \ldots\ldots 3d^{10}, 4p^0\rangle$

**Cu (II)** as $\cos\Theta\,|1s^2 \ldots\ldots 3d^9, 4p^0\rangle$

$-\sin\Theta\,|1s^2 \ldots\ldots 3d^{10}\underline{L}, 4p^0\rangle$

$\underline{L}$ denotes that the covalency gives a partial $\underline{2p}$ character to the $\underline{d}$ hole

- Final states $|1s^1 \ldots\ldots 4p^1\rangle$

Antibonding $\sigma^*$

Non-bonding $\pi^*$

In the cluster approach, the ground state of square planar cuprates the admixture of configurations:

- $\alpha_0\,|3d^9\rangle + \beta_0\,|3d^{10}\underline{L}\rangle$,

with $\alpha_0^2+\beta_0^2=1$ and $\alpha_0^2>\beta_0^2$, because of the divalent character

A more explicit way of writing the admixture of configurations

- $\alpha_0\,|Cu.1s^2\ldots3d^9, O\ 1s^2\ldots2p^6\rangle + \beta_0\,|Cu.1s^2\ldots3d^{10}, O\ 1s^2\ldots2p^5\rangle$

Etat fondamental




- Etats excités

L.E Basse E. → $|f_1\rangle = +\alpha_f\,|\underline{c}\ldots3d^{(9)}\ldots e_k\rangle + \beta_f\,|\underline{c}\ldots3d^{(10)}\underline{L}\ldots e_k\rangle$ — dominant, $\beta_f^2 >> \alpha_f^2$ — $I_1$

H.E Haute E. → $|f_2\rangle = -\beta_f\,|\underline{c}\ldots3d^{(9)}\ldots e_k\rangle + \alpha_f\,|\underline{c}\ldots3d^{(10)}\underline{L}\ldots e_k\rangle$ — dominant — $I_2$

with $\alpha_f^2+\beta_f^2=1$ ($e_k$ represents the photoelectron with a wavevector **k**).

Cu K → $4p^1$

**XPS** $e_K \rightarrow$ ▷ (9-10eV)

**Cu K XAS** $e_K \rightarrow 4p^1$ $(mp^1)$ — 2 TRANSITIONS $|f_1\rangle$ & $|f_2\rangle$ @ diff energies (6-7eV)

- $L_{III}, L_I$ XAS — 1 TRANSITION $|\ldots 3d^{10}\rangle$
  $\neq$
  $L_{III}, L_{II}$ XPS — 2 TRANSITIONS $|f_1\rangle$ $|f_2\rangle$

- $O_K$
  $1s \rightarrow 2p$ $\quad |f\rangle = |\ldots 2p^6\rangle$

$L_{III}$ ≠ XPS $\left(W = \left[(U_{cd}-\Delta)^2 + 4T^2\right]^{1/2}\right.$ $\left.\frac{I_2}{I_1} = \tan^2(\theta'-\theta)\right)$

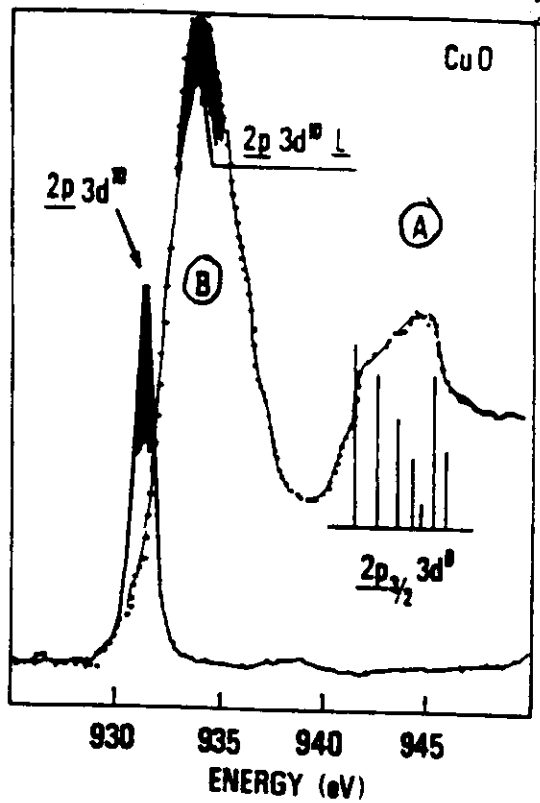


De Santis Bianconi Lagarde Flank et al. (1987)

final state

- $L_{III}$ $\quad |\ldots 2p^{3/2} \ldots 3d^{10} \ldots\rangle$
  ≤
- XPS $\quad f_1 = \cos\theta' \,|\underline{c}\, 3d^9\rangle - \sin\theta' \,|\underline{c}\, 3d^{10}\underline{L}\rangle$ (B)
  $f_2 = \sin\theta' \,|\underline{c}\, 3d^9\rangle + \cos\theta' \,|\underline{c}\, 3d^{10}\underline{L}\rangle$ (A)
  ( + $e^-$ delocal… )

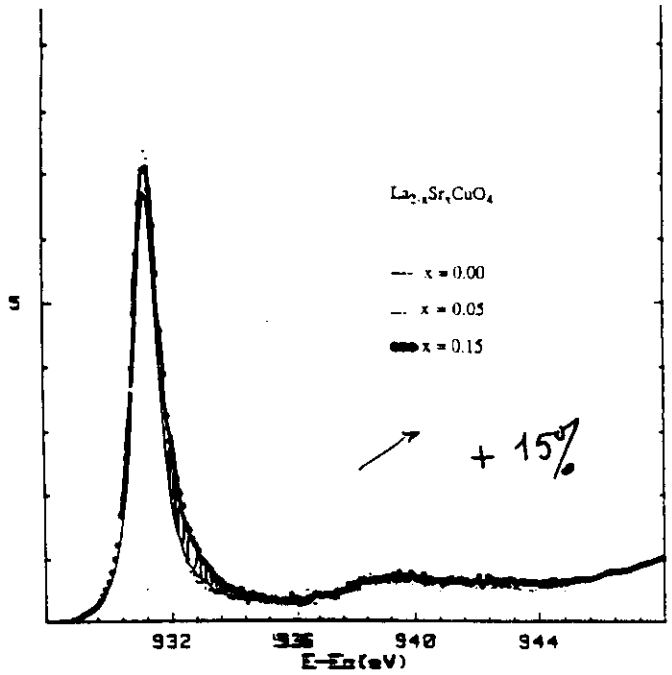


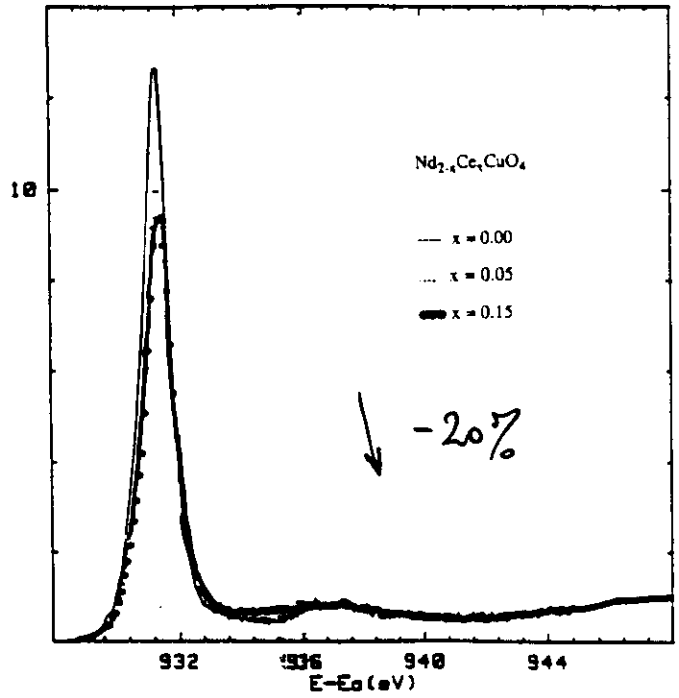


H. Tolentino et al. To be published Physica C

$$\Delta = E(3d^{10}\underline{L}) - E(3d^9)$$

$$= \langle 3d^{10}\underline{L} | H | 3d^{10}\underline{L} \rangle - \langle 3d^9 | H | 3d^9 \rangle$$

- En fait H non ionique $\begin{vmatrix} 0 & 0 \\ 0 & \Delta \end{vmatrix}$

  mais H iono covalent $\begin{vmatrix} 0 & T \\ T & \Delta \end{vmatrix}$

$\Rightarrow$ nouvelles valeurs propres $E = \frac{1}{2}\Delta \pm \frac{1}{2}\sqrt{\Delta^2+4T^2}$

nouveaux vecteurs propres

Etat fondamental

$$|1\rangle = \cos\theta \, |1s^2 \ldots 3d^9\rangle - \sin\theta \, |1s^2 \ldots 3d^{10}\underline{L}\rangle$$

$$\operatorname{tg} 2\theta = \frac{2T}{\Delta}$$ cuprates $\Rightarrow \cos^2\theta \sim 0.7$

- Etats finals

$T' \simeq T$ $\quad \langle 3d^{10}\underline{L} | H | 3d^9 \rangle$

$$H = \begin{vmatrix} 0 & T' \\ T' & \Delta - U_{\underline{c}d} \end{vmatrix}$$

$$\operatorname{tg} 2\theta' = \frac{2T'}{\Delta - U_{\underline{c}d}}$$

$$|f_1\rangle = \cos\theta' \, |\underline{c} \ldots 3d^9 \ldots e_K\rangle - \sin\theta' \, |\underline{c} \ldots 3d^{10}\underline{L} \, e_K\rangle$$

$$|f_2\rangle = \sin\theta' \quad + \cos\theta'$$

$$\frac{I_2 \text{ (satellite)}}{I. \text{ principal}} = \frac{|\langle i | f_2 \rangle|^2}{|\langle i | f_1 \rangle|^2} = \frac{\cos\theta\sin\theta' - \sin\theta\cos\theta'}{\cos\theta\cos\theta' + \sin\theta\sin\theta'} = \operatorname{tg}(\theta' - \theta)$$

# Comment changer le mélange

- INITIAL $|i\rangle = \cos\theta\,|\ 3d^9\rangle - \sin\theta\,|\ \ldots 3d^{10}\underline{L}\rangle$

$$tg\,2\theta = \frac{2T}{\Delta} > 0 \qquad 0 < 2\theta < 90° \qquad 0 < \theta < 45°$$

- FINAL $|f_1\rangle = |\cos\theta' \quad -\sin\theta'|\ |\underline{c}\,.\,d^9 \ldots e_k\rangle$

$|f_2\rangle = |\sin\theta' \quad +\cos\theta'|\ |\underline{c}\,.\,d^{10}\underline{L} \ldots e_k\rangle$

| | $\Delta$ | T | $U_{cd}$ | W | $\cos^2\theta$ | $\sin^2\theta'$ | $I_2/I_1$ | W |
|---|---|---|---|---|---|---|---|---|
| XPS (2p) | 1.5 | 2 | 9 | 4.3 | 0.67 | 0.94 | 0.76 | 8.5 |
| XAS (1s) | 1.5 | 2 | 6 | 4.3 | 0.67 | 0.87 | 0.47 | 6 |

$$I_2/I_1 = tg^2(\theta' - \theta)$$

$$W = \left[(\Delta - U_{cd})^2 + 4T^2\right]^{1/2}$$

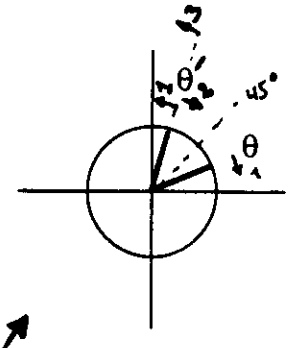


1) $\Delta \nearrow$ : W ↘ $I_2/I_1$ ↗

2) $U_{cd} \searrow$ : W ↘ $I_2/I_1$ ↘

3) $T \uparrow \downarrow$ : W ↘ $I_2/I_1$ ↗

Si $\Delta' = 2T$ $\theta' = 31.7°$

//

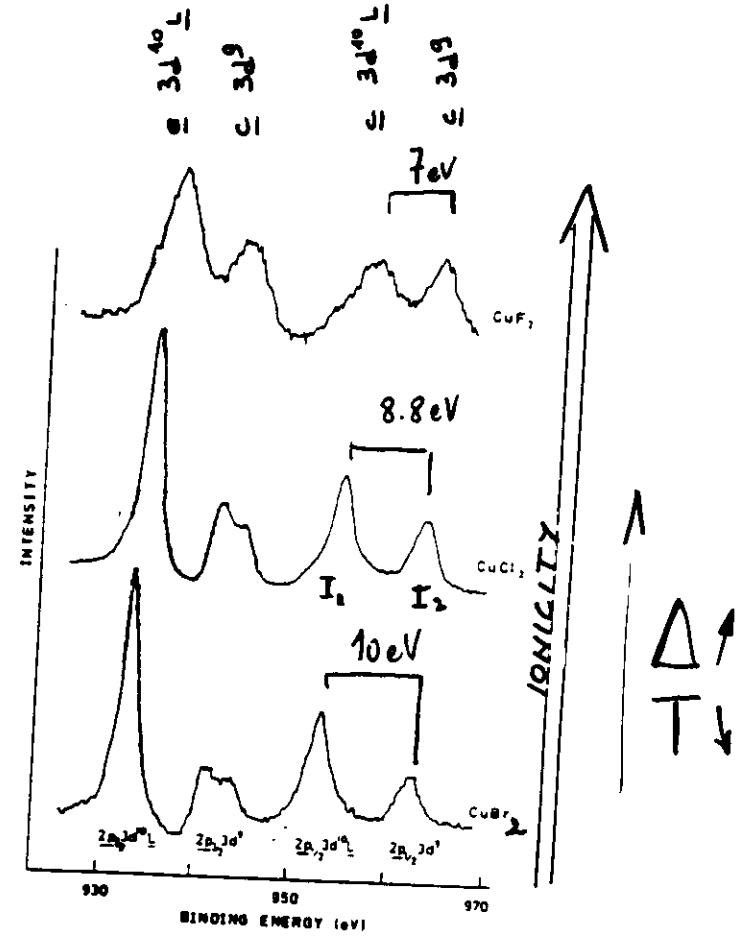


Van der Laan
XPS
PRB. 1981

Fig.6 Spectres de photoémission d'électrons (XPS) des halogénures de cuivre $CuF_2$, $CuBr_2$, $CuCl_2$ [d'après G.van der Laan et al-1981].

$\Delta \uparrow \rightarrow$ $W \downarrow \left[(U_{cd} - \Delta)^2 + 4T^2\right]^{1/2}$

$\frac{I_2}{I_1} \nearrow$ $tg^2(\theta' - \theta)$

$\theta' \uparrow, \theta \downarrow$

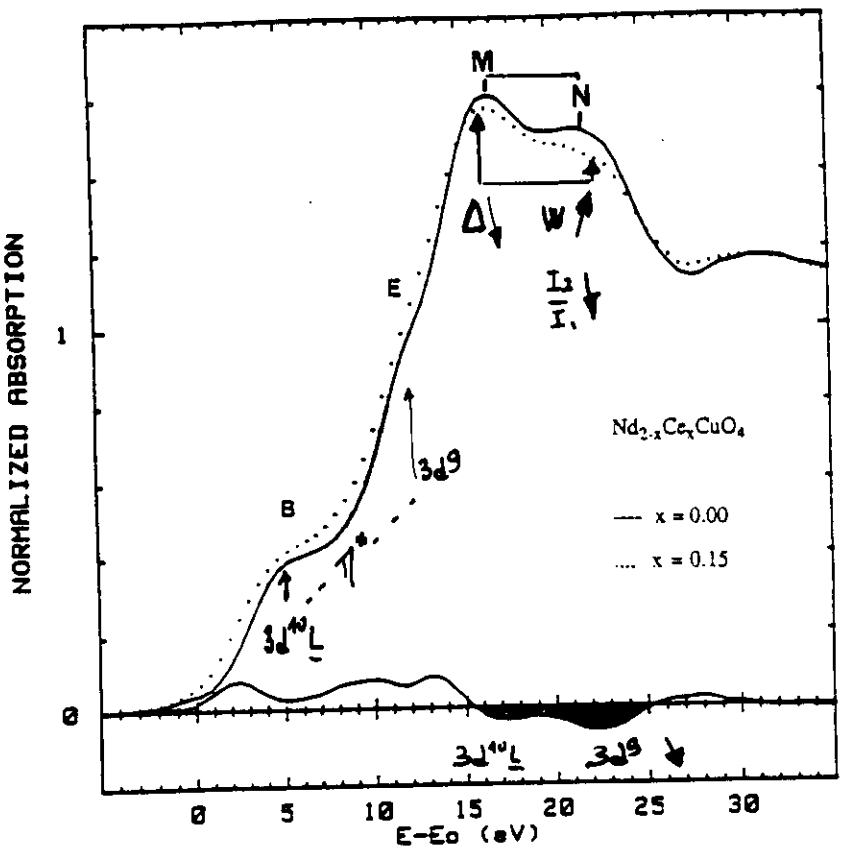


Fig. 3 Cu K-edge spectrum of $Nd_{2-x}Ce_xCuO_4$ for x=0 and x=0.15. The difference between the spectra evidences that the weight of the $3d^{10}\underline{L}$ configuration (B and M) increases under doping, leading to a decrease of the weight of the $3d^9$ configuration (E and N).

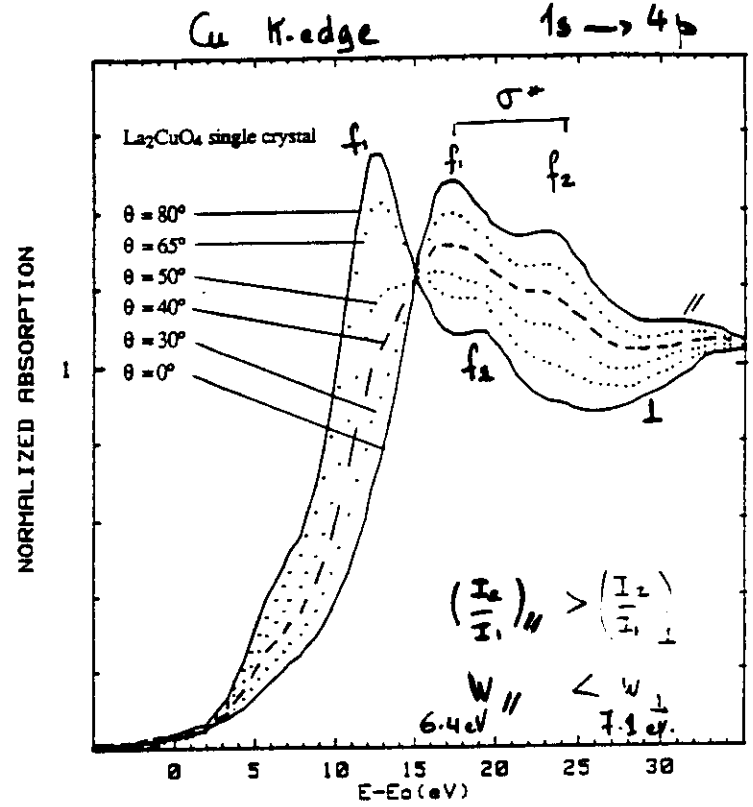


Fig. 2 Angle-resolved Cu K-edge XAS spectra of $La_2CuO_4$ single crystal. Apart from an energy re-scaling to account for differences in next neighbor distances, the anisotropy of the relative intensity of the $3d^{10}\underline{L}$ and $3d^9$ transitions is induced by the symmetry of the photoelectron wavevector k relative to the O $2p_{x,y}$ ligand electron.

$e_K^{\perp}$ ~ "XPS"

$e_K^{//}$ ~ "screening actor"

Cu K-edge ① —> MULTICHANNEL
2 XANES , 2 EXAFS

② —> SCREENING
↓
SYMMETRY of the
PHOTOELECTRON

d = 7.4 eV ⊥ $e_k^{\perp}$ Spectator "~ XPS"
= 1.5eV ($4p_z^1$)
~ 2eV W ~ 7.1eV

// $e_k^{//}$ actor at Low ENERGY W ~ 6.4eV.
// ~ 1.25eV

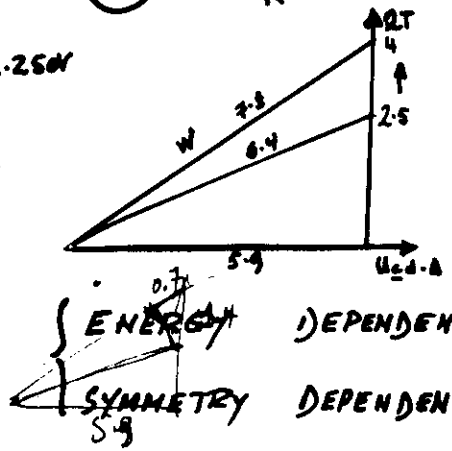


- reduce $3d^{10}\underline{L}$

at HIGH ENERGY
(⇒ "~ XPS"

{ ENERGY DEPENDENCE
SYMMETRY DEPENDENCE } OF THE RESPECTIVE WEIGHT.

XAS d Cu K edge LUCKY Cu $^{0\ hole}_{1\ hole}$

$Cu^{II}\ O^{--}$

- INITIAL STATE

$\cos\theta\ |3d^9\rangle - \sin\theta\ |3d^{10}\underline{L}\rangle$

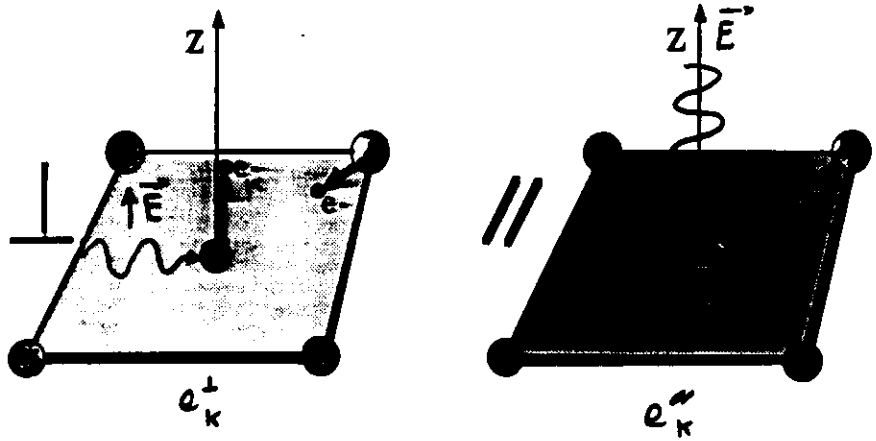


- FINAL STATE ($3d^{10}\underline{L}$)

$\cos\theta'_{\perp}$ ; $\sin\theta'_{\perp}$ $\cos\theta'_{//}$ ; $\sin\theta'_{//}$

Interaction $e_k$ ; $a_T^-$

⇒ ANISOTROPY $\theta'_{\perp} \neq \theta'_{//}$

$\sin^2\theta'_{\perp} > \sin^2\theta'_{//}$

Fig.1 Schematical view for the origin of the anisotropy of the relaxation in the final state of square planar $CuO_2$. The photoelectron deposited with low kinetic energy in orbitals perpendicular to the square plane (e.g. $4p_z^*$) does not interfere with the charge-transfer process taking place in the planes, contrary to the photoelectron put into in-plane orbitals (e.g. $4p_{x,y}^*$).

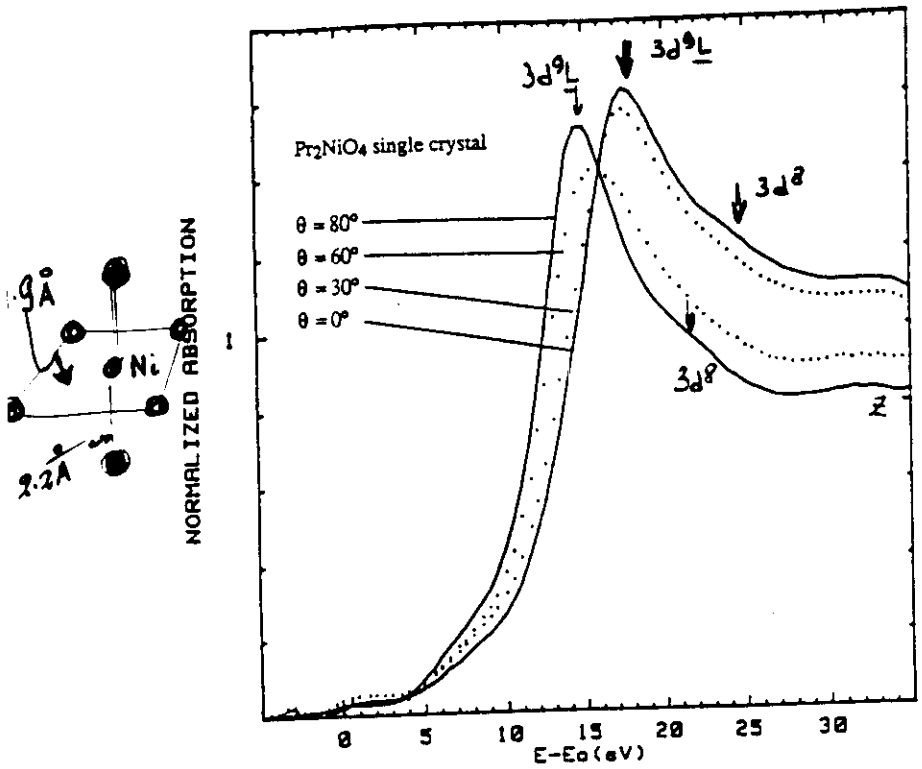


Fig.3 Angle-resolved Ni K-edge XAS spectra of $Pr_2NiO_4$. Apart for a contraction of the energy scale due to slightly different distances along x,y and z directions, one can observe that the dominant configuration is the fully relaxed one for both orientations, conversely to what happens in cuprates.

2 holes
$\underline{d}_{x^2-y^2}$
$\underline{d}_{3z^2-r^2}$

$Ni^{II}$

$Pr_2Ni_4O$ " good octahedron. "

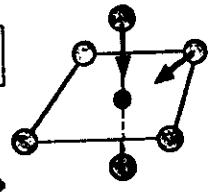

Initial st. $\alpha\,|3d^8\,2p^6\rangle + \beta\,|3d^9\,2p^5\rangle$

Final st. $\alpha^c_{//,\perp}|c\ 3d^8\,2p^6\,e_{//,\perp}\rangle + \beta^c_{//,\perp}|c\ 3d^9\,2p^5\,e_{//,\perp}\rangle$

× No Anisotropy

· Full. relaxed $3d^9\underline{L}$ dominant

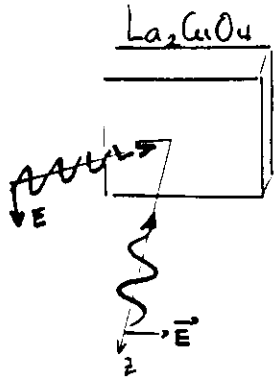


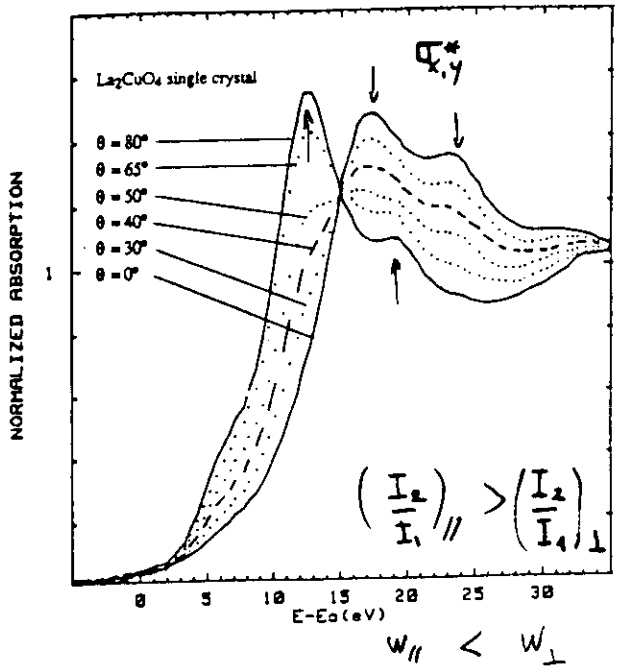


Initial state $\alpha\,|3d^9\,2p^6\rangle + \beta\,|3d^{10}\,2p^5\rangle$

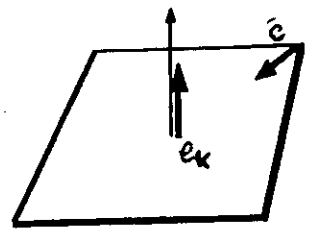


$\perp$ ≈ PHOTOEMISSION

Final state $\alpha^c_{\perp}|c\ 3d^9\,2p^6\,e_{\perp}\rangle + \beta^c_{\perp}|c\ 3d^{10}\,2p^5\,e_{\perp}\rangle$

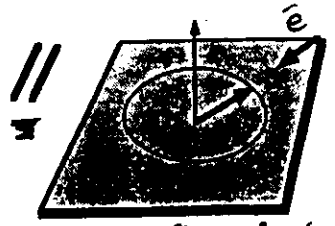


Interaction

Final state $\alpha^c_{//}|c\ 3d^9\,2p^6\,e_{//}\rangle + \beta^c_{//}|c\ 3d^{10}\,2p^5\,e_{//}\rangle$

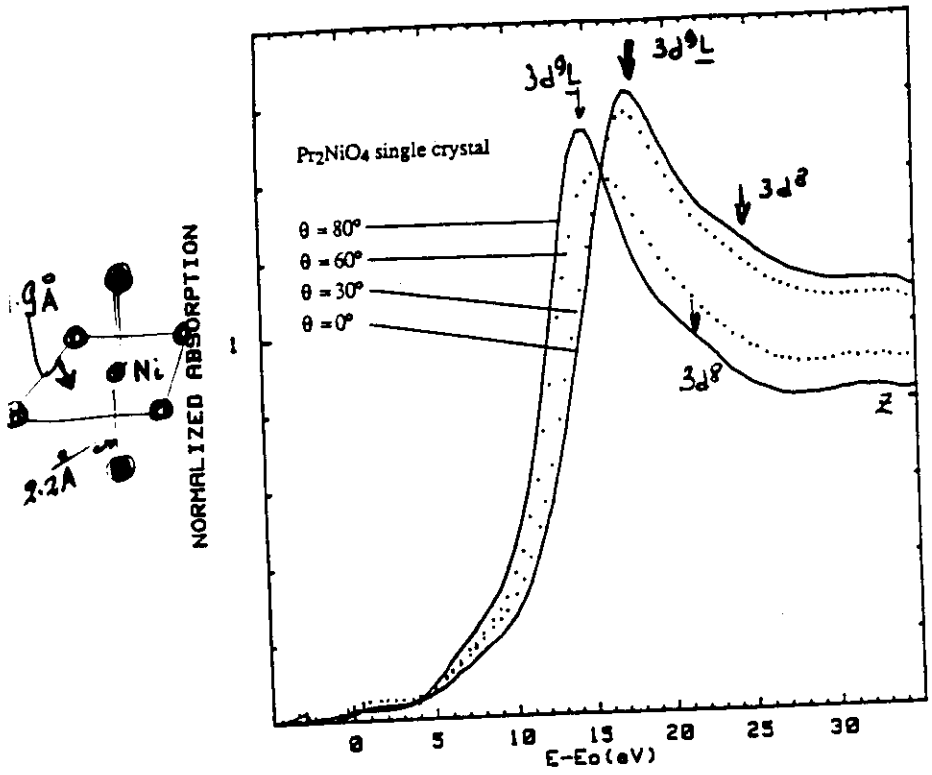


Fig.3 Angle-resolved Ni K-edge XAS spectra of $Pr_2NiO_4$. Apart for a contraction of the energy scale due to slightly different distances along x,y and z directions, one can observe that the dominant configuration is the fully relaxed one for both orientations, conversely to what happens in cuprates.

2 holes
$d_{x^2-y^2}$
$d_{3z^2-r^2}$

$Ni^{II}$

$Pr_2Ni_4O$ " good octahedron. "

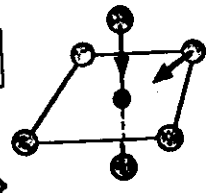

Initial st. $\alpha\,|3d^8\,2p^6\rangle + \beta\,|3d^9\,2p^5\rangle$

Final st. $\alpha^c_{//,\perp}\,|c\;3d^8\,2p^6\,\underline{e}_{//,\perp}\rangle + \beta^c_{//,\perp}\,|c\;3d^9\,2p^5\,\underline{e}_{//,\perp}\rangle$

× No Anisotropy

$3d^9\underline{L}$ dominant

## 5 - Cu K XAS versus XPS

The major difference between XPS and XAS deals with the status of the photoelectron $e_k$.

- In XPS, the photoelectron goes to the vacuum, with a large kinetic energy.

K-edge: In XAS, it stays in the probed material, with a low kinetic energy when the photon comes just with the very threshold energy.

- In Cu 2p XPS, one observes two lines, a lorentzian-like main line $|1s^2..2p...3d^{10}\underline{L}..e_k\rangle$ and a satellite $|1s^2..2p...3d^9..e_k\rangle$.

- **Cu K-edge XAS signal ≈ a convolution of the two lines found in XPS times the Cu partial density of states**

**(XAS ≈ XPS⊗Cu mp-DOS : m = 4, 5, ...).**

The convolution with the 4p states, the lowest lying ones, gives rise to the resolved double features mentionned above. The transitions to mp (m>4) appears as a continuum.

### Photoelectron and its symmetry

The wavevector **k** has to be specified perpendicular ($k_\perp$) or parallel ($k_{//}$) to the square planar unit, according to the direction of the polarization of the incident photon.

In the final state admixture of configurations

$$\alpha_f|\underline{c}..3d^9..e_k\rangle + \beta_f|\underline{c}..3d^{10}\underline{L}..e_k\rangle,$$

$k_\perp$ and $k_{//}$ leads to ($\alpha_{f\perp}$ and $\beta_{f\perp}$) and ($\alpha_{f//}$ and $\beta_{f//}$).

No need for "shake-down", "shake-up"

Key-word Admixture of Configurations

**XAS ≈ XPS ⊗ 4 (m) p DOS ⊗ "photoelectron"**

⇒ **2 EXAFS or (4 for powders)**

$$// \quad \& \quad \perp$$

$$3d^{10}\underline{L} \;\&\; 3d^{9}$$

$$\alpha_{//}(E) \qquad \& \qquad \beta_{//}(E)$$

$$\alpha_{\perp}(E) \qquad \& \qquad \beta_{\perp}(E)$$

⇒ **needs for single crystal data**

**Multichannel problems are very general**

**" Linear and Circular Dichroisms"**

**Photons ↑ or → create different X A Spectra**